

bradscholars

Mold temperature- and molar mass-dependent structural formation in micro-injection molding of isotactic polypropylene

Item Type	Article
Authors	Zhao, X.;Liao, T.;Yang, X.;Coates, Philip D.;Whiteside, Benjamin R.;Barker, D.;Thompson, Glen P.;Jiang, Z.;Men, Y.
Citation	Zhao X, Liao T, Yang X et al (2022) Mold temperature- and molar mass-dependent structural formation in micro-injection molding of isotactic polypropylene. Polymer. 248: 124797.
DOI	https://doi.org/10.1016/j.polymer.2022.124797
Publisher	Elsevier
Rights	© 2022 Elsevier Ltd. All rights reserved. Reproduced in accordance with the publisher's self-archiving policy. This manuscript version is made available under the CC-BY-NC-ND 4.0 license.
Download date	2025-07-16 13:08:10
Link to Item	http://hdl.handle.net/10454/19031

Mold temperature- and molar mass-dependent structural formation in micro-injection molding of isotactic polypropylene

Xintong Zhao ^{a,b}, Tao Liao ^a, Xiao Yang ^c, Phil Coates ^d, Ben Whiteside ^d, David Barker ^d, Glen Thompson ^d, Zhiyong Jiang ^{a,*}, Yongfeng Men ^{a,b,**}

a State Key Laboratory of Polymer Physics and Chemistry, Changchun Institute of Applied Chemistry, Chinese Academy of Sciences, Renmin Street 5625, Changchun, 130022, PR China

b School of Applied Chemistry and Engineering, University of Science and Technology of China, Hefei, 230026, PR China

c Research Institute of Maoming Petrochemical Company, SINOPEC, Maoming, 525000, PR China

d Faculty of Engineering and Informatics, University of Bradford, Bradford, BD7 1DP,

Abstract

The structural formation and development of isotactic polypropylene (iPP) upon the micro-injection molding process was investigated at different mold temperatures and molecular weights utilizing a real-time synchrotron radiation small angle X-ray scattering (SAXS) technique combined with a customized micro-injection molding apparatus. Shish-kebab structure and parent-daughter lamellae were found to be formed during micro-injection molding for all iPP samples. In the case of kebab lamellae, a considerable growth in the long period and in the average thickness of lamellar crystallites and amorphous domains is observed at initial stages of crystallization for samples molded at varying temperatures. This effect is caused by the successive formation of thin lamellae in the outer layer and thick lamellae in the inner layer during the manufacturing process as evidenced by the spatial distribution of the crystalline lamellae across the thickness. In addition, the length of the shish formation increases remarkably at the onset of crystallization, the extent of which is dependent on the mold temperature. Despite the large changes of the lamellar stacks and the shish misorientation, the final length of the shish remains essentially unchanged when varying mold temperature. Since there is a critical orientation molecular weight above which the chains are stretched and oriented to form stable shish, the iPP sample with a low molar mass exhibits an overall decrease in the scattering intensity of SAXS patterns compared to the high molecular weight polypropylene.

1. Introduction

A large number of polymer resins can only be used after being shaped to the resultant products by means of various processing techniques. Generally, polymer materials start in a molten state and then are machined into final products under the effect of shear flow during the manufacturing process. These facts mean that the flow is an unavoidable factor, and the microstructure of products is affected by the processing methods and conditions to a large extent. As a result, many studies have paid close attention to the flow-induced crystallization (FIC) events during the shaping process. After decades of research, three major points of FIC have been elucidated. First, at the nucleation stage, the flow field can accelerate the crystallization by increasing the nucleation rate by an order of magnitude [1–3]. Second, the flow could induce different crystal modifications of the polymer, e.g., isotactic polypropylene forms the β crystal under the effect of the shear flow field [4–8]. Third, the strong flow field changes the crystal morphology of polymers, i.e., transformation from spherulites to oriented lamellae or even to shish-kebab structures [9–12]. Shish-kebab structures can greatly improve the mechanical properties of polymer materials. Its discovery sets off the prelude to the study of FIC, and its formation mechanism has always been the core problem in FIC. Li et al. systematically summarized that the formation of shish is a multistep process [13]. The flow-induced local order forms the primary nuclei along the flow direction, and the flow-induced needle-like precursor grows from these primary nuclei to form a shish structure [14]. Another case is that a large amount of primary nucleus accumulation gathers to form oriented nuclei and eventually grows into a shish structure [10]. In addition, Keller et al. improved the concept of the coil-stretch transition (CST) for polymers under a flow field [15,16]. The CST indicated that there was a window range when the strain rate reached a critical value and the coil-stretch transition started. However, because CST was derived from a polymer solution system, it was not fully applicable to polymer melt systems. Therefore, Pennings et al. proposed a stretched network model that considered that the primary nuclei of shish structures stemmed from the stretched networks [17–19]. Moreover, Hsiao et al. accomplished extensive studies of the formation mechanisms of shish-kebab structures [12,20–27]. By examining the *in situ* crystallization process of polymer melts (e.g., polypropylene, polyethylene, and their blends) under shear flow field, they found that high molar mass chains can significantly accelerate the crystallization kinetics of the whole system to form a shish-kebab structure [20,21,23,27]. The higher the content of high molar mass chains, the faster the crystallization kinetics during the flow-induced crystallization process accompanied by the higher degree of orientation and the larger number of oriented crystals [26]. Furthermore, the degree of crystal orientation and the crystallization kinetics rose with the enhancement of

both strain rate and strain, while at the same strain, a short shear time at a high speed was more effective than a long shear time at a low speed [28].

Based on the above concepts, numerous studies have focused on real time investigations of the structural formation and development during the manufacturing process [18,23,29–34], especially in the injection molding process. For example, Bubeck et al. [35,36] studied the level of orientation of chain segments in liquid crystalline polymers under the filling phase using a customized injection molding apparatus. Yang et al. employed in-cavity temperature profiles to unravel the solidification kinetics upon injection molding of high-density polyethylene [37] and its blend with polypropylene [38]. With the fast advance in microelectromechanical systems (MES) in recent years [39,40], micro-injection molding (μ IM) is being extensively applied in micro- and nanoscale component manufacture [41–43]. Differently from the conventional injection molding, μ IM possesses an extremely high injection velocity and pressure, a strong shearing field, and a fast cooling rate [44, 45]. The flow visualization of the filling process and the structure of μ IM molded samples have been reported by numerous studies [46–48]. Nevertheless, few investigations have placed emphasis on the *in situ* structural formation during the course of micro-injection molding [13]. To enable the study of the nanoscale structure evolution in a micro-injection molding process, a portable device was specifically developed for time resolved measurement activities [49]. In this study, we chose isotactic polypropylene (iPP) sample as a model system because of its broad applicability, and the structural evolution of iPP samples under micro-injection molding was studied at varying mold temperatures and molecular weights using synchrotron small angle X-ray scattering (SAXS) technique. The results revealed how the characteristic features of shish formation and kebab lamellae are affected by the processing parameters and molecular architecture.

2. Experimental section

2.1. Sample characteristics

Two isotactic polypropylene materials were purchased from Aldrich Polymer Products: iPP190K ($M_w = 190\,000$ g/mol and $M_w/M_n = 3.8$) and iPP340K ($M_w = 340\,000$ g/mol and $M_w/M_n = 3.5$). The molar mass distribution features of these two samples were characterized utilizing a PL-GPC 220 high-temperature GPC (Polymer Laboratories Ltd.) at 150 °C. In addition, the rheological properties of the polymer melts at 200 °C were measured by means of an ARES-G2 rheometer (TA Instruments, America). The iPP granules were injection molded into rectangular bars via a homemade micro-injection molding device. The configuration and specifications of this unique device developed in house were described in detail in ref. 49. The samples were fabricated at three selected mold temperatures of 80, 100, and 120 °C. The melt temperature and the plunger velocity were chosen at 200 °C and 14.3 mm/s [49], respectively. Fig. 1 shows the samples at the position of diamond X-ray windows used for thermal analysis and multiscale structure characterization.

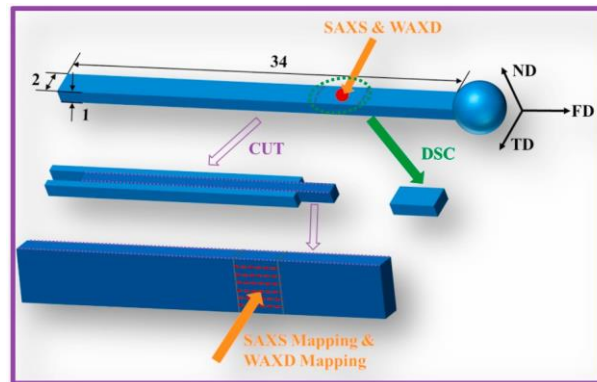


Fig. 1. Schematic illustration of the micro-injection molded polypropylene sample with a dimension of $34 \times 2 \times 1$ mm³ for SAXS, WAXD, and DSC measurements.

2.2. SAXS measurement

Real time synchrotron small angle X-ray scattering experiments were implemented at beamline BL19U2 at SSRF, Shanghai, China. The wavelength of the X-ray beam was 0.09184 nm, and the beam size at the sample position was 200×35 μ m². An exposure time of 0.03 s and a time interval of 0.003 s for each SAXS pattern were adopted to achieve a high time resolution during the micro-molding process. The SAXS patterns were registered using a Pilatus 1 M detector (981 pixels \times 1043 pixels with a pixel size of 172×172 μ m²), and the distance between the sample and the detector was 2345 mm. Subsequently, SAXS mapping experiments

after the injection molding process were performed utilizing a Rigaku NANOPIX WAXD/SAXS system equipped with a copper rotary target. The wavelength of the X-ray radiation was 0.154 nm, and the dimension of the incident X-ray beam at the sample position was set as $200 \times 200 \mu\text{m}^2$. The sample-to-detector distance was 1306 mm, and the X-ray beam scanned along the thickness direction at a step length of $200 \mu\text{m}$. The SAXS patterns were collected with an exposure time of 120 s by a Rigaku Hypix 6000 detector ($771 \text{ pixels} \times 1179 \text{ pixels}$ with a pixel size of $100 \mu\text{m}$).

2.3. WAXD measurement

Wide angle X-ray diffraction experiments were conducted on a custom-designed microfocus X-ray diffraction system of Xenocs with an X-ray radiation wavelength of 0.154 nm. The dimension of the X-ray radiation at the sample position was $40 \times 60 \mu\text{m}^2$. Each WAXD pattern was recorded within 300 s at a sample-to-detector distance of 68 mm using a Pilatus 100 K detector ($487 \text{ pixels} \times 195 \text{ pixels}$). On the other hand, the structural distributions were probed by scanning over half the thickness of the rectangular strips with steps of 0.1 mm via WAXD mapping experiments.

2.4. DSC experiment

DSC thermograms were obtained from a DSC1 Star[®] system of Mettler Toledo under a N_2 atmosphere. The samples for thermal analysis were cut from the middle of the rectangular bar and sealed in aluminum pans. Melting thermograms were obtained by heating the samples up from 25 to $200 \text{ }^\circ\text{C}$ at a scanning rate of 10 K/min .

3. Results and discussion

3.1. Influence of the mold temperature on structural formation

The structural developments of iPP340K samples upon the micro-injection molding process are given in Fig. 2 at varying crystallization times and mold temperatures.

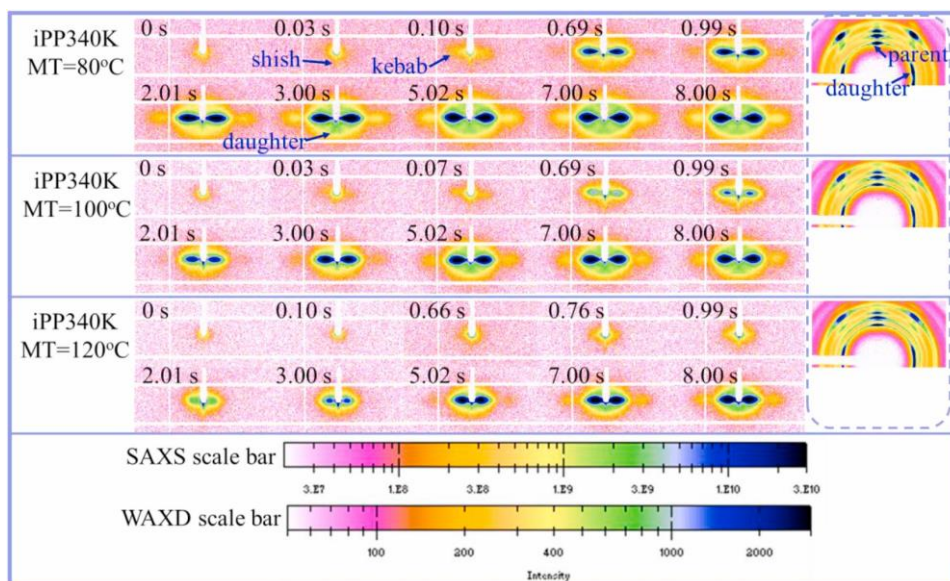


Fig. 2. Selected 2D-SAXS patterns (left) taken at varying times as indicated on each profile during the micro-injection molding process and 2D-WAXD patterns (right) after the micro-injection molding process of the samples at different mold temperatures. The flow direction is horizontal.

The polypropylene pellets were shaped at selected mold temperatures of 80, 100, and $120 \text{ }^\circ\text{C}$ under a melt temperature of $200 \text{ }^\circ\text{C}$. The first pattern ($t = 0 \text{ s}$) was obtained just before the polymer melt reached the diamond window. Subsequently, the melt subjected to the shear flow field passed through the diamond window, and the detector started to acquire the scattering signal of the sample. For all three samples, the signal of a typical shish-kebab structure is observed from SAXS patterns. Furthermore, one finds relatively weak scattering maxima in the meridional direction, meaning the generation of a fraction of correlated lamellae whose normals are vertical to the injection molding direction. In addition, 2D-WAXD patterns were obtained at room temperature after molding, and the results confirm an oriented parent-daughter lamellae structure. Moreover, the content of β -crystals is found to increase with

increasing mold temperature due to the effect of shear flow field as shown in Figs. S1–S3. These observations can be explained by the fact that the long chains are partially oriented and aligned in the molding direction to form the shish structure first under a strong shear flow field, then the shish formation accelerates primary nucleation and growth of crystallites in which the molecular chain direction is also parallel to the molding direction producing the kebab structure [50,51], and finally the daughter lamellae with the polymer chains aligned perpendicular to the flow direction crystallize onto the kebab crystals. The onset times of these structural formations are displayed in Fig. 3. As the mold temperature is elevated, the presence of these ordered structures is found to be delayed evidently, which is due to the growing chain mobility at higher mold temperatures [52]. High temperature not only leads to rapid relaxation of molecular chains and reduces the chain orientation to suppress the formation of shish structures, but also increases the time for molecular chains to align into lamellae.

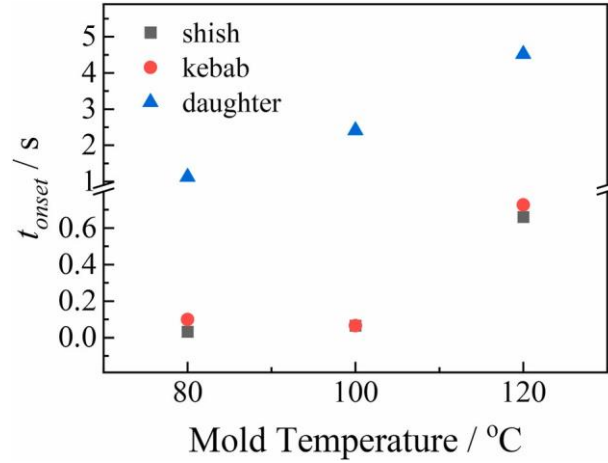


Fig. 3. Onset time of the formation of shish, kebab, and daughter lamellae structures measured at different mold temperatures.

The scattering invariant Q can be used to qualitatively represent the evolution of ordered structures upon the injection molding process. The value of Q can be obtained as follows [53]:

$$Q = \int_{q_{min}}^{q_{max}} \int_{q_{min}}^{q_{max}} I(q_x, q_y) dq_x dq_y \propto \varphi_s (1 - \varphi_s) (\rho_s - \rho_a)^2 \quad (1)$$

where φ_s represents the volume fraction of the scatterer, and the ρ_s and ρ_a are the average electron densities of the scatterer and the surrounding matrix, respectively. The scattering invariant is, therefore, determined by the relative volume fraction of the scatterers and the electron density difference between the phases in iPP. In this work, the Q values of the shish structure (Q_{shish}), daughter lamellae structure ($Q_{daughter}$), and kebab crystals (Q_{kebab}) were acquired by integrating the scattering intensity of the corresponding structures along the meridional and equatorial directions, respectively, and the results are shown in Fig. 4.

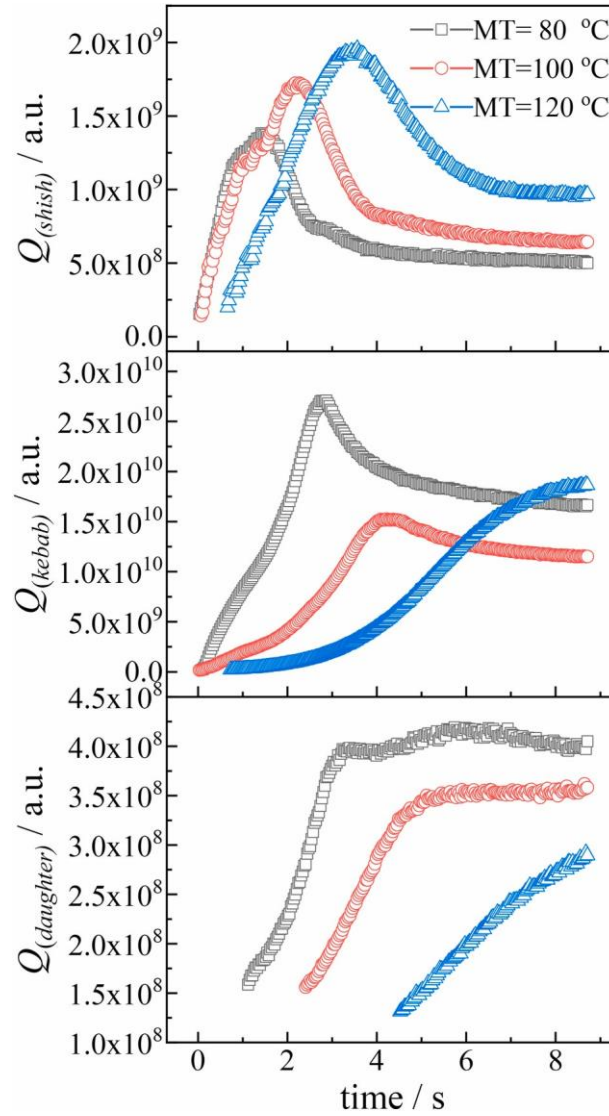


Fig. 4. Change of the scattering invariant of different structures (from top to bottom: shish structure, kebab structure, and daughter lamellae structure) with crystallization time.

In the case of shish structure, the change of the scattering invariant with time behaves in a similar manner for samples molded at different temperatures. The integrated scattering intensity increases dramatically at first, and then reaches a maximum value followed by a distinct reduction. These observations are attributed to a growth of the volume fraction of the shish formation induced by the strong shear field and a relaxation of the oriented chains that originally constitute the shish after cessation of shear, respectively. As the mold temperature is increased, the scattering invariant exhibits a greater value at late stages of crystallization because the molecular chains underwent a longer shear time at higher mold temperatures, thus leading to the generation of the shish structure with a higher content. Regarding the kebab lamellae, the integrated scattering intensity shifts to smaller values at long crystallization times for samples molded at 80 and 100 °C, indicating the occurrence of more defective crystallites and a reduction in the electron density difference upon crystallization. In the micro-injection molding process, the melt filled the cavity and solidified into lamellae at high temperature, and then the temperature of the whole sample cooled rapidly down to the preset mold temperature after a relatively short time. On the other hand, there is a continuous increase in the scattering invariant for the sample molded at 120 °C within the limited time range of experimental observations due to slow crystallization of polymeric chains into kebab crystals at such high temperature. For the daughter lamellae, the scattering invariant increases rapidly at the beginning and reaches a plateau. Meanwhile, one notes an overall decrease in $Q_{daughter}$ as the mold temperature is raised, which is mainly due to a decrease in the volume fraction of the daughter lamellae.

To assess the development of kebab and daughter lamellae during crystallization, SAXS scattering intensity distribution curves were acquired by narrow fan-shaped integration within $\pm 10^\circ$ along the equatorial and meridional directions, respectively. Fig. 5 displays SAXS profiles of the samples with different mold temperatures after Lorentz correction.

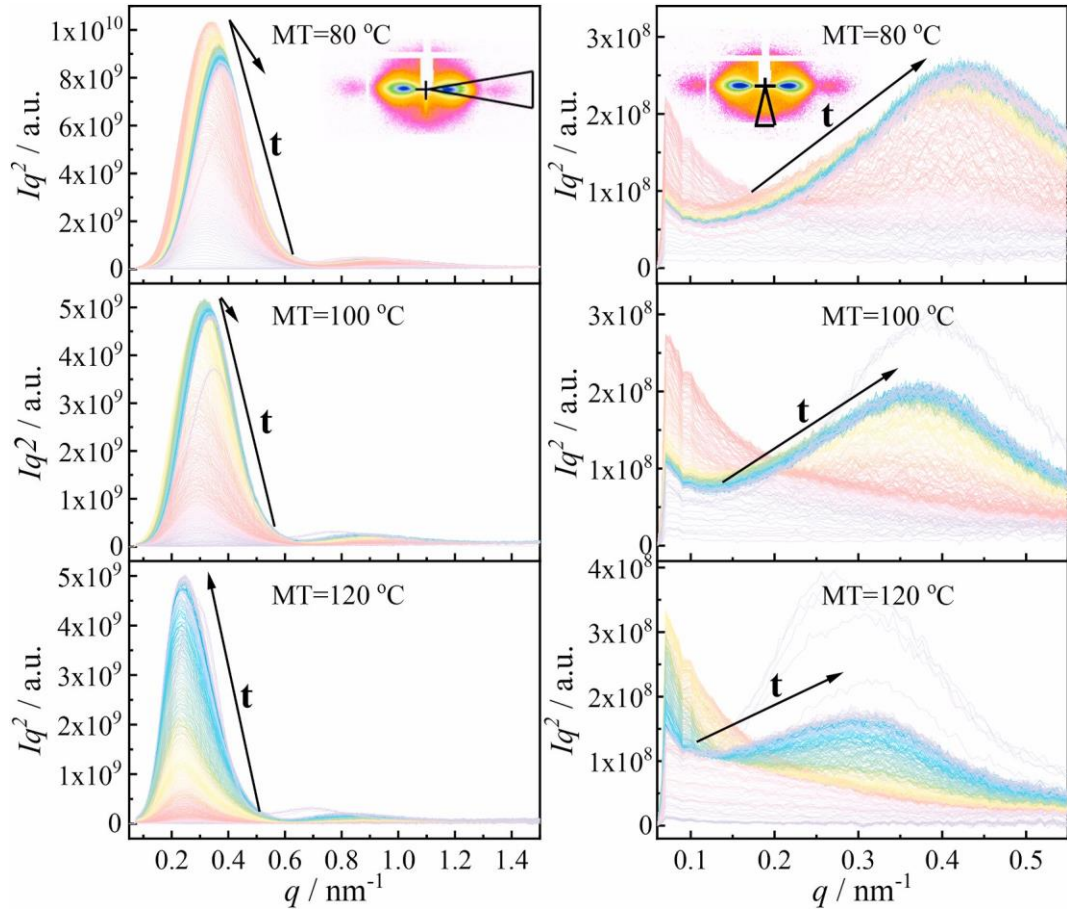


Fig. 5. SAXS scattering intensity distribution curves taken along the equatorial direction (left) and meridional direction (right) at varying times and mold temperatures. The insets of the figures show how the scattering intensity distribution curves are obtained.

It should be noted that Lorentz correction is applicable for the isotropic samples whereas no Lorentz correction should be applied for the highly oriented structures. Because the molded samples possess a multilayer structure with different degree of orientations, there is no unique recipe for data treatment in this case. As a result, Lorentz-corrected data were chosen in the present work. Moreover, the long period (d_{ac}), the lamellar thickness (d_c), and the amorphous domain thickness (d_a) were derived from the correlation function $K(z)$ [54–58]:

$$K(z) = \frac{\int_0^{\infty} I(q)q^2 \cos(qz) dq}{\int_0^{\infty} I(q)q^2 dq} \quad (2)$$

The resultant correlation functions $K(z)$ are presented in the Fig. S6. The variations in d_{ac} , d_c , and d_a for kebab lamellae with crystallization time are demonstrated in Fig. 6. Since the crystallinities of iPP340K samples are lower than 50% as determined from the DSC data in Fig. S7, the amorphous phase thickness d_a can be extracted from the expression $d_a = d_{ac} - d_c$. It is obvious that the changes in d_{ac} , d_c and d_a with crystallization time demonstrate a similar characteristic feature for samples molded at different mold temperatures. The long period $d_{ac(kebab)}$ exhibits a remarkable increase at the onset of crystallization followed by a plateau value and then decreases gradually to a stable value. The initial increase can be attributed to the formation of the outer layer at low temperature and the inner layer at high temperature in sequence. The melt flows into the cavity and crystallizes rapidly near the cavity wall, thus producing lamellae with a smaller d_{ac} . Due to the thermal insulation and heat preservation effect of the outer layer, the polymer melt in the inner part crystallizes at a temperature higher than the mold temperature thus forming thicker lamellar crystals. This fact is also evidenced by the gradual increase in the lamellar thickness at the initial stage of crystallization. As the melt is cooled down to the mold temperature, the generation of thinner and defective lamellae in the subsequent crystallization process results in a decrease of the long period. For comparison, the plots of d_{ac} , d_c , and d_a for daughter lamellae are presented against crystallization time in Fig. 7.

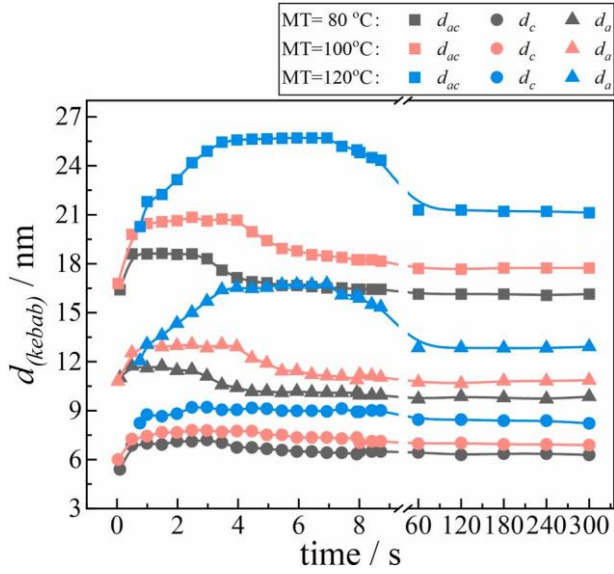


Fig. 6. Change of d_{ac} , d_c , and d_a of the kebab lamellae with crystallization time taken at different mold temperatures.

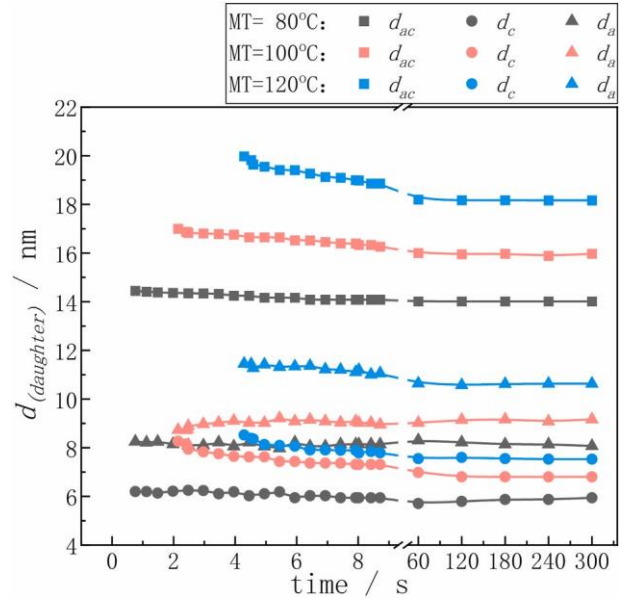


Fig. 7. Change of d_{ac} , d_c , and d_a of the daughter lamellae with crystallization time taken at different mold temperatures.

It is found that the three structural parameters of the daughter crystals decrease steadily until an essentially constant value is reached. This behavior is due to the formation of thin daughter lamellae during cooling down to the corresponding mold temperature.

Furthermore, the average length L_{shish} and the misorientation B_ϕ of the shish formation can be assessed from azimuthal scattering intensity distributions of the meridional scattering streak employing the Ruland equation as follows [59]:

$$B_{abs} = \left(\frac{1}{L_{shish}} \frac{2\pi}{q} \right) + B_\phi \quad (3)$$

where B_{obs} denotes the integral breadth of the azimuthal scattering intensity distribution, and B_ϕ represents the misorientation of the shish. As a result, L_{shish} and B_ϕ can be derived from the slope and the intercept of the linear fitting curve of B_{obs} versus $1/q$ (as shown in Fig. S9), respectively. The results of the shish length and the shish misorientation are given in Figs. 8 and 9.

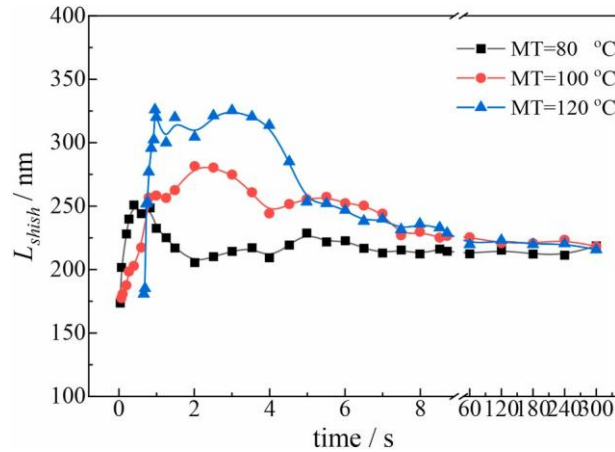


Fig. 8. Change of the length of the shish with crystallization time measured at varying mold temperatures.

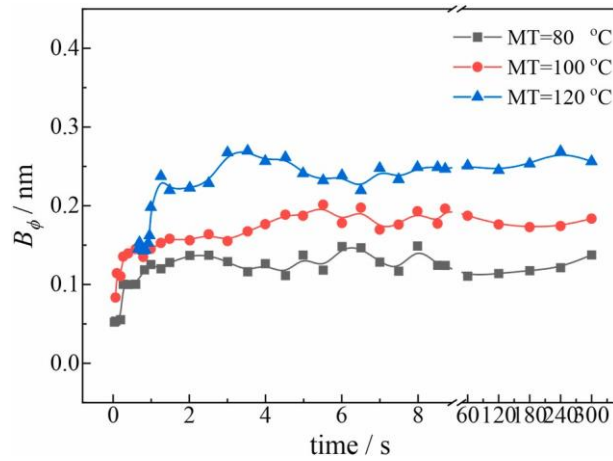


Fig. 9. Change of the shish misorientation with time measured at varying mold temperatures.

The values of both L_{shish} and B_ϕ increase apparently at the beginning of shear-induced crystallization, reflecting a growth of the shish formation with a low extent of orientation along the injection molding direction. This phenomenon is in agreement with the automatic catalytic effect [49,60,61]. A portion of the molecular chains could diffuse to the tip of the shish structure under the driving force of the difference in the free-energy between the nucleus formed by the flow-sheared melt and the surrounding undercooled melt. Since the new molecular chains that are incorporated into the shish possess a smaller degree of orientation, the increase in the shish length is accompanied by a decline in the average degree of orientation. Subsequently, the length of shish reaches a plateau value followed by a remarkable decrease whereas the shish orientation remains almost unchanged during further crystallization. Because a fraction of shish structures are thermally unstable, the relaxation of oriented molecular chains in the shish results in a reduction of the average shish length after shear flow. Another significant issue to be noted is the influence of mold temperature on the dimension and orientation of the shish structure. On one hand, the value of B_ϕ increases evidently with the increase of the mold temperature due to mobile chain segments at high temperature. On the other hand, the average length of shish rises dramatically with increasing mold temperature at early stages of crystallization. This phenomenon is due to the fact that the polymer melt experiences a long shear time at high mold temperature during the micro-molding process due to low undercooling. However, the value of L_{shish} is basically not affected by the mold temperature at the final stage of crystallization, which is due to the same content of long chains that can form the stable shish structure for the molded samples [27,62].

3.2. Multilayer structure of micro-injection molded iPP

Many studies have corroborated that injection molded samples are generally composed of skin layer and core layer [63–65]. To reveal the multilayer structure of the molded samples in this work, SAXS and WAXD experiments scanned along the thickness direction of samples. Fig. 10 collects SAXS and WAXD patterns at varying positions over the thickness of samples molded at different temperatures.

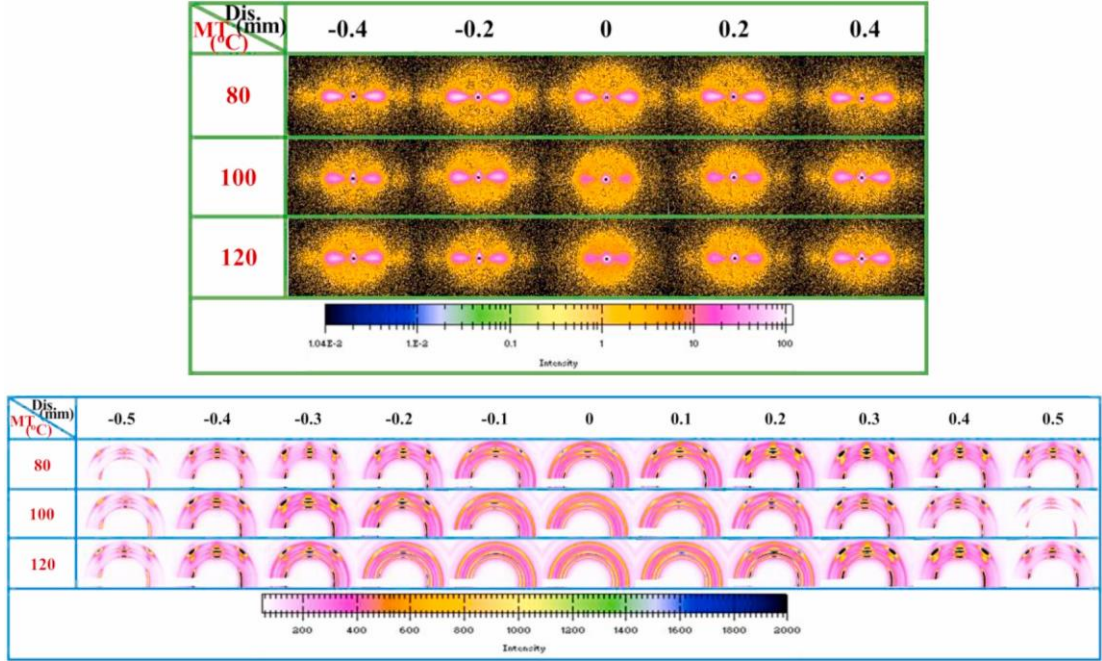


Fig. 10. Selected 2D-SAXS (top) and 2D-WAXD (bottom) patterns along the thickness direction of samples molded at different temperatures of 80, 100, and 120 °C. The distance from the center of the sample is marked on the graph.

There is no core layer for all three samples as evidenced by the anisotropic intensity distributions of the SAXS and WAXD patterns across the thickness.

Furthermore, the extent of the polymer chain orientation can be assessed with the following equation [66]:

$$S_{hkl} = \frac{3 \langle \cos^2 \varphi_{hkl} \rangle - 1}{2} \quad (4)$$

where $\cos^2 \varphi_{hkl}$ was obtained from the azimuthal scattering intensity distribution $I_{hkl}(\varphi)$ using the following relation:

$$\langle \cos^2 \varphi_{hkl} \rangle = \frac{\int_0^{\pi} I_{hkl}(\varphi) \sin \varphi \cos^2 \varphi d\varphi}{\int_0^{\pi} I_{hkl}(\varphi) \sin \varphi d\varphi} \quad (5)$$

and φ can be evaluated utilizing the Polanyi equation [67]:

$$\cos \varphi_{hkl} = \cos \theta_{hkl} \cos \psi \quad (6)$$

where φ_{hkl} , θ_{hkl} , and ψ are the angle between the normal vector of the (hkl) reflection and the injection molding direction, the Bragg diffraction angle, and the azimuthal angle, respectively. Fig. 11 demonstrates the extent of orientation of the $(040)_a$ reflection at different positions.

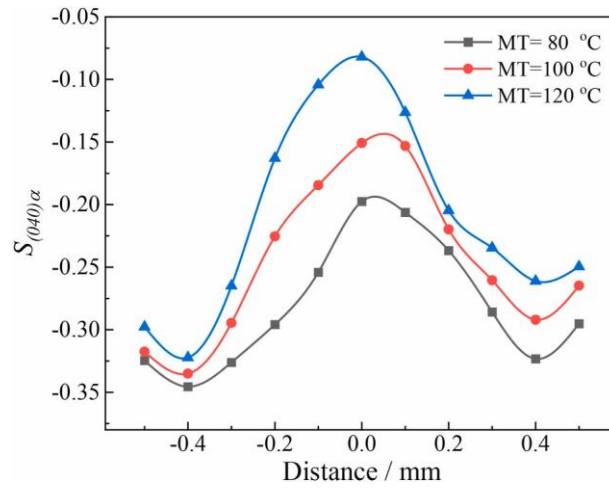


Fig. 11. Variations of $S_{(040)\alpha}$ at different thickness positions measured for samples with varying mold temperatures.

One finds the orientation of the chain segments across the whole sample thickness. The occurrence of the maximum orientation at positions of ca. ± 0.4 mm can be interpreted by the fact that fast cooling of the polymer melt close to the cavity wall gives rise to a frozen layer at which the molecular chains have insufficient time to align along the injection molding direction. Therefore, the shear rate close to the sample edge is enhanced because of a reduction in the cavity cross-sectional area. In addition, the overall level of orientation reduces with the increase of mold temperature, which is mainly because high temperature facilitates the relaxation of oriented molecular chains.

Moreover, Fig. 12 presents the evolution of d_{ac} , d_c , and d_a of the kebab structure along the thickness direction at different mold temperatures. It is noted that the values of these three parameters in the inner layer are definitely larger than those in the outer layer, and the higher the mold temperature is, the larger the d_{ac} and d_c . Because there is a temperature gradient over the sample thickness, the molecular chains in the inner layer crystallize at high temperature leading to the formation of thick lamellar stacks. These findings are well identical to the results that the value of d_c for the kebab lamellae increases notably at the initial stages of crystallization in Fig. 6.

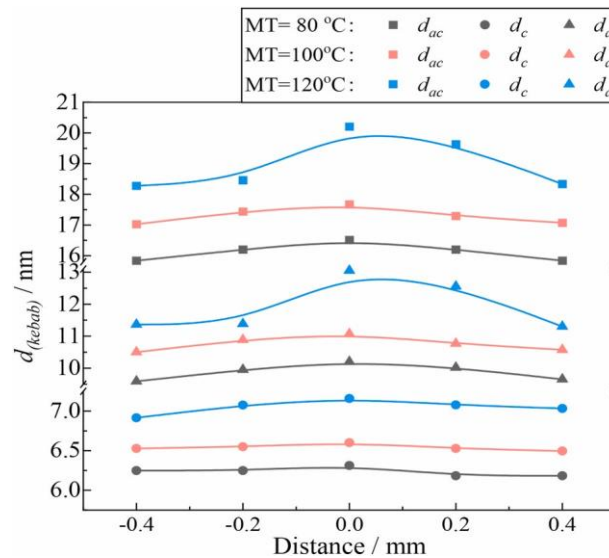


Fig. 12. Variations of d_{ac} , d_c , and d_a of kebab structure along the thickness direction of samples with different mold temperatures.

3.3. Influence of the molecular weight on structural formation

Another iPP190K sample with a low molecular weight was employed to clarify the effect of molecular weight on the structural formation during the micro-injection molding process. Fig. 13 shows SAXS diagrams of iPP190K sample at varying crystallization times.

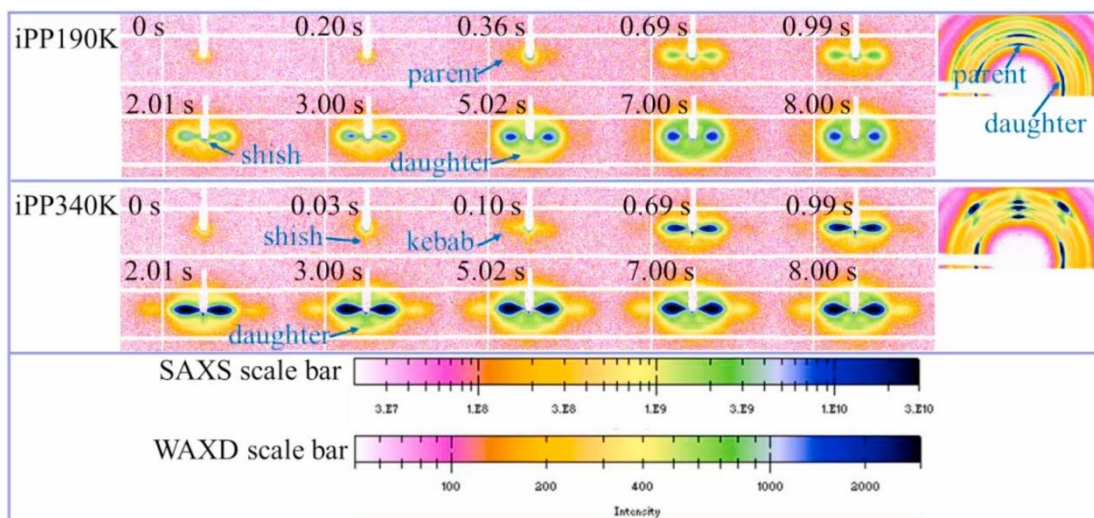


Fig. 13. SAXS diagrams of iPP samples with varying molecular weights taken at various crystallization times. WAXD patterns are collected at room temperature after micro-injection molding as demonstrated in the right plot of the figure. The mold temperature and the melt temperature are 80 °C and 200 °C, respectively. The plunger velocity is 14.3 mm/s.

The SAXS patterns of iPP340K sample are also displayed in the figure for the sake of comparison. Shish formation and parent-daughter lamellae are also observed in the case of iPP190K sample. Nevertheless, one notes an overall decrease of the scattering intensity for the iPP190K compared to the iPP340K at corresponding times. GPC measurements were performed to reveal the molecular characteristics of these two samples, and the molecular weight distributions of both iPP190K and iPP340K are shown in Fig. 14.

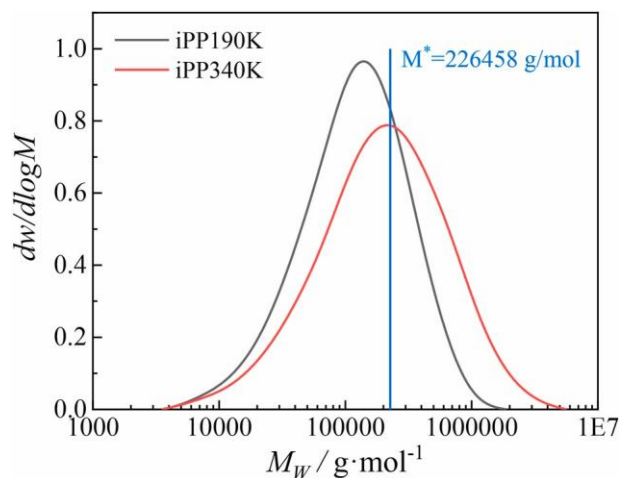


Fig. 14. Molecular weight distribution profiles of two samples with different molecular weights. The blue line shows the critical orientation molecular weight under a plunger velocity of 14.3 mm/s. (For interpretation of the references to colour in this figure legend, the reader is referred to the Web version of this article.)

Furthermore, the rheological properties of the two samples were determined by parallel plate geometries, and the results are given in Fig. 15.

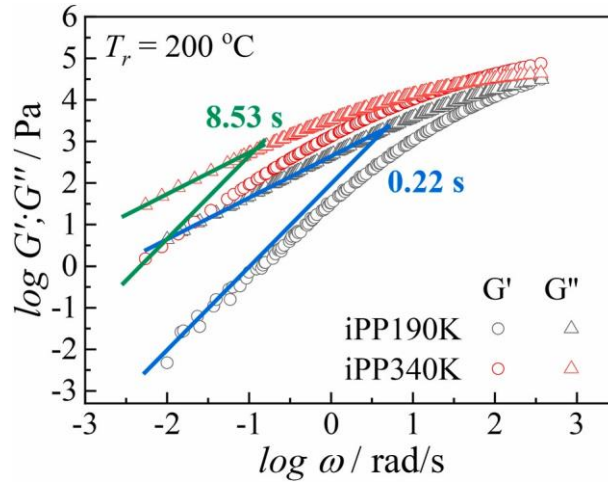


Fig. 15. Rheological properties of two iPP materials with different molecular weights recorded at 200 °C.

The reptation times (τ_d) of the iPP190K and iPP340K materials at 200 °C are approximately 0.22 s and 8.53 s, respectively. Based on the relation $\tau_R = \tau_d (M_e/M_w)^{1-1.5}$ [68,69], where M_e represents the molar mass between entanglement points and $M_e = 6850$ g/mol for the present system [70], the Rouse times (τ_R) is calculated to be approximately 7.93×10^{-3} s and 0.17 s for iPP190K and iPP340K, respectively. It is obvious that the molecular chains of iPP190K are more likely to relax to the random coil. In addition, the apparent shear rate $\dot{\gamma}$ of the polymer melt is calculated to be 1213 s^{-1} via the relation $\dot{\gamma} = 6Q/(WH^2)$ [71]. Since $\dot{\gamma}$ is much larger than τ_R^{-1} , the molecular chains of the two samples could be stretched to form an oriented structure. It was reported that molecular weight and its distribution play critically important roles in determining the crystallization rate and resultant morphology during the shearing process [72]. Hsiao et al. obtained a scaling expression between the critical orientation molar mass (M^*) and the shear rate, which is expressed as $M^* = 6.57 \times 10^5 \times \dot{\gamma}^{-0.15}$ [73]. Hence, the critical orientation molecular weight M^* is approximately 226,458 g/mol under the plunger velocity of 14.3 mm/s described in this work, and M^* is shown by the blue line in Fig. 14. Only when the molecular weight of chains is larger than M^* can the molecular chains be arranged into shish structures along the flow direction under a shear flow field. For iPP190K sample, the content of chains with a high molecular weight is significantly lower than that for iPP340K. Consequently, only a small fraction of the chains in iPP190K sample are stretched and oriented to form shish and kebab lamellae upon the molding process compared to iPP340K sample, leading to a reduction of the scattering intensity of SAXS patterns.

On the basis of the above observations, shish formation, kebab crystals, and daughter lamellae of samples with different molecular weights occur sequentially, as represented schematically in Fig. 16. When the melt is subjected to a strong shear flow field during the micro- injection molding process, some longer molecular chains are aligned along the flow direction to form shish structures, which subsequently provide the growth sites for the kebab lamellae. The daughter lamellae whose molecular chains are oriented perpendicular to the flow direction are generated at approximately 80° to the kebab lamellae at late stages of micro-injection molding.

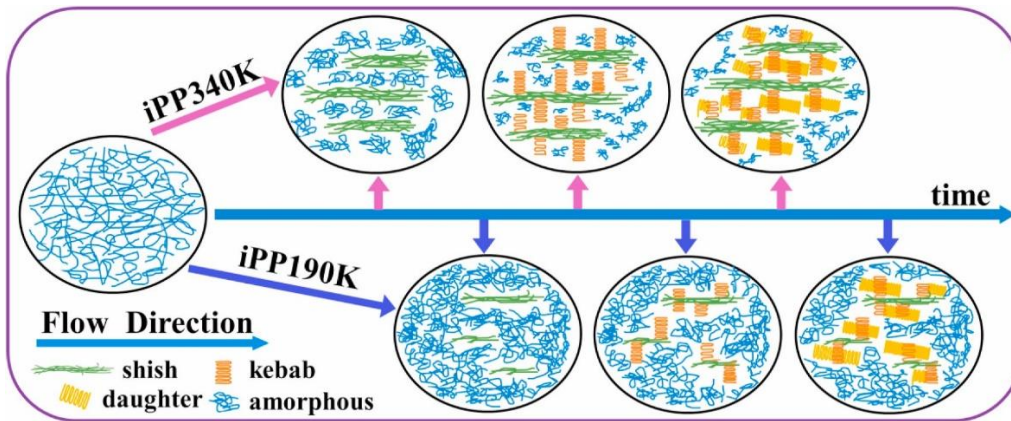


Fig. 16. Schematic illustration of the formation of the shish-kebab structure and parent-daughter lamellae structure for samples with different molar masses under micro-injection molding

4. Conclusions

The formation and evolution of shish and parent-daughter structures in iPP samples with different mold temperatures and molecular weights were investigated at varying times using an *in situ* synchrotron SAXS technique combined with a homemade micro-injection molding instrument. For kebab lamellae, the long period increases dramatically at early stages of crystallization, which is due to crystallization temperature gradient across the thickness of molded samples. This effect is also evidenced by the formation of thin lamellar stacks in the outer layer and thick lamellar stacks in the inner layer. However, the long period of daughter lamellae decreases continuously until an essentially constant value is reached, which is attributed to the generation of thin daughter lamellae upon cooling down to the mold temperature. In addition, one observes a considerable growth of the shish length at the onset of crystallization, the extent of which depends on the mold temperature. In spite of the large variations in the lamellar thickness, amorphous layer thickness, and misorientation of shish, the final shish length was found to be independent of mold temperature. Because of only a small fraction of chains with the molar mass higher than the critical orientation molar mass M^* , the iPP190K sample exhibits an overall reduction of the scattering intensity at corresponding crystallization times compared to the iPP340K.

Declaration of competing interest

The authors declare that they have no known competing financial interests or personal relationships that could have appeared to influence the work reported in this paper.

Acknowledgments

This work is financially sponsored by the National Key R&D Program of China (2018YFB0704200), National Natural Science Foundation of China (21674119, 21790342 and 51525305), and Royal Society Newton Advanced Fellowship, United Kingdom (NA150222). X. Z. thanks Prof. Hai Wang at Dalian University of Technology for his kind assistance in the SAXS mapping experiments.

Appendix A. Supplementary data

Supplementary data to this article can be found online at <https://doi.org/10.1016/j.polymer.2022.124797>.

References

- [1] R.S. Graham, Modelling flow-induced crystallisation in polymers, *Chem. Commun.* 50 (2014) 3531–3545.
- [2] F.G. Hamad, R.H. Colby, S.T. Milner, Onset of flow-induced crystallization kinetics of highly isotactic polypropylene, *Macromolecules* 48 (2015) 3725–3738.
- [3] H. Janeschitz-Kriegl, E. Ratajski, Kinetics of polymer crystallization under processing conditions: transformation of dormant nuclei by the action of flow, *Polymer* 46 (2005) 3856–3870.
- [4] X.W. Li, Y.M. Mao, H.Y. Ma, F. Zuo, B.S. Hsiao, B. Chu, An *in-situ* X-ray scattering study during uniaxial stretching of ionic liquid/ultra-high molecular weight polyethylene blends, *Polymer* 52 (2011) 4610–4618.
- [5] Y. Chen, G. Zhong, J. Lei, Z. Li, B.S. Hsiao, *In situ* synchrotron X-ray scattering study on isotactic polypropylene crystallization under the coexistence of shear flow and carbon nanotubes, *Macromolecules* 44 (2011) 8080–8092.
- [6] D. Zhou, S.G. Yang, J. Lei, B.S. Hsiao, Z.M. Li, Role of stably entangled chain network density in shish-kebab formation in polyethylene under an intense flow field, *Macromolecules* 48 (2015) 6652–6661.
- [7] T.B. van Erp, L. Balzano, G.W.M. Peters, Oriented gamma phase in isotactic polypropylene homopolymer, *ACS Macro Lett.* 1 (2012) 618–622.
- [8] M. Zhou, S. Xu, Y. Li, C. He, T. Jin, K. Wang, H. Deng, Q. Zhang, F. Chen, Q. Fu, Transcrystalline formation and properties of polypropylene on the surface of ramie fiber as induced by shear or dopamine modification, *Polymer* 55 (2014) 3045–3053.
- [9] J.K. Keum, Y. Mao, F. Zuo, B.S. Hsiao, Flow-induced crystallization precursor structure in high molecular weight isotactic polypropylene (HMW-iPP)/low molecular weight linear low density polyethylene (LMW-LLDPE) binary blends, *Polymer* 54 (2013) 1425–1431.
- [10] H. Janeschitz-Kriegl, E. Ratajski, M. Stadlbauer, Flow as an effective promotor of nucleation in polymer melts: a quantitative evaluation, *Rheol. Acta* 42 (2003) 355–364.
- [11] Y. Liu, Z. Hong, L. Bai, N. Tian, Z. Ma, X. Li, L. Chen, B.S. Hsiao, L. Li, A novel way to monitor the sequential destruction of parent-daughter crystals in isotactic polypropylene under uniaxial tension, *J. Mater. Sci.* 49 (2014) 3016–3024.

- [12] R.H. Somani, L. Yang, L. Zhu, B.S. Hsiao, Flow-induced shish-kebab precursor structures in entangled polymer melts, *Polymer* 46 (2005) 8587–8623.
- [13] K.P. Cui, Z. Ma, N. Tian, F.M. Su, D. Liu, L.B. Li, Multiscale and multistep ordering of flow-induced nucleation of polymers, *Chem. Rev.* 118 (2018) 1840–1886.
- [14] G. Eder, H. Janeschitzkriegl, S. Liedauer, Crystallization processes in quiescent and moving polymer melts under heat-transfer conditions, *Prog. Polym. Sci.* 15 (1990) 629–714.
- [15] M.H. Nafar Sefiddashti, B.J. Edwards, B. Khomami, Communication: a coil-stretch transition in planar elongational flow of an entangled polymeric melt, *J. Chem. Phys.* 148 (1974), 141103.
- [16] A. Keller, H.W. Kolnaar, Flow-induced Orientation and Structure Formation, *Materials science and technology*, 2006, pp. 189–268.
- [17] J. Smook, J. Pennings, Influence of draw ratio on morphological and structural- changes in hot-drawing of uhmw polyethylene fibers as revealed by DSC, *Colloid Polym. Sci.* 262 (1984) 712–722.
- [18] K.P. Cui, Z. Ma, Z. Wang, Y.X. Ji, D. Liu, N.D. Huang, L. Chen, W.H. Zhang, L.B. Li, Kinetic process of shish formation: from stretched network to stabilized nuclei, *Macromolecules* 48 (2015) 5276–5285.
- [19] Y. Ogino, H. Fukushima, G. Matsuba, N. Takahashi, K. Nishida, T. Kanaya, Effects of high molecular weight component on crystallization of polyethylene under shear flow, *Polymer* 47 (2006) 5669–5677.
- [20] B.S. Hsiao, L. Yang, R.H. Somani, C.A. Avila-Orta, L. Zhu, Unexpected shish-kebab structure in a sheared polyethylene melt, *Phys. Rev. Lett.* 94 (2005) 117802.
- [21] J.K. Keum, F. Zuo, B.S. Hsiao, Formation and stability of shear-induced shish-kebab structure in highly entangled melts of UHMWPE/HDPE blends, *Macromolecules* 41 (2008) 4766–4776.
- [22] L. Yang, R.H. Somani, I. Sics, B.S. Hsiao, R. Kolb, H. Fruitwala, C. Ong, Shear- induced crystallization precursor studies in model polyethylene blends by in-situ rheo-SAXS and rheo-WAXD, *Macromolecules* 37 (2004) 4845–4859.
- [23] F. Zuo, J.K. Keum, L. Yang, R.H. Somani, B.S. Hsiao, Thermal stability of shear- induced shish-kebab precursor structure from high molecular weight polyethylene chains, *Macromolecules* 39 (2006) 2209–2218.
- [24] R.H. Somani, L. Yang, B.S. Hsiao, P.K. Agarwal, H.A. Fruitwala, A.H. Tsou, Shear- induced precursor structures in isotactic polypropylene melt by *in-situ* rheo-SAXS and rheo-WAXD studies, *Macromolecules* 35 (2002) 9096–9104.
- [25] R.H. Somani, B.S. Hsiao, A. Nogales, H. Fruitwala, S. Srinivas, A.H. Tsou, Structure development during shear flow induced crystallization of i-PP: *In situ* wide-angle X- ray diffraction study, *Macromolecules* 34 (2001) 5902–5909.
- [26] R.H. Somani, L. Yang, B.S. Hsiao, Effects of high molecular weight species on shear- induced orientation and crystallization of isotactic polypropylene, *Polymer* 47 (2006) 5657–5668.
- [27] A. Nogales, B.S. Hsiao, R.H. Somani, S. Srinivas, A.H. Tsou, F.J. Balta-Calleja, T. A. Ezquerro, Shear-induced crystallization of isotactic polypropylene with different molecular weight distributions: *in situ* small- and wide-angle X-ray scattering studies, *Polymer* 42 (2001) 5247–5256.
- [28] R.H. Somani, L. Yang, B.S. Hsiao, T. Sun, N.V. Pogodina, A. Lustiger, Shear-induced molecular orientation and crystallization in isotactic polypropylene: effects of the deformation rate and strain, *Macromolecules* 38 (2005) 1244–1255.
- [29] P.E. Lopes, M.S. Ellison, W.T. Pennington, *In situ* X-ray characterisation of isotactic polypropylene during melt spinning, *Plast. Rubber Compos.* 35 (2013) 294–300. [30] M. van Drongelen, D. Cavallo, L. Balzano, G. Portale, I. Vittorias, W. Bras, G. C. Alfonso, G.W.M. Peters, Structure development of low-density polyethylenes during film blowing: a real-time wide-angle X-ray diffraction study, *Macromol. Mater. Eng.* 299 (2014) 1494–1512.
- [31] K. Cui, Y. Liu, L. Meng, X. Li, Z. Wang, X. Chen, L. Li, A novel apparatus combining polymer extrusion processing and x-ray scattering, *Polym. Test.* 33 (2014) 40–47. [32] L.P. Meng, Y.F. Lin, J.L. Xu, X.W. Chen, X.Y. Li, Q.l. Zhang, R. Zhang, N. Tian, L. B. Li, A Universal equipment for biaxial stretching of polymer films, *Chin. J. Polym. Sci.* 33 (2015) 754–762.
- [33] Q.L. Zhang, L.F. Li, F.M. Su, Y.X. Ji, S. Ali, H.Y. Zhao, L.P. Meng, L.B. Li, From molecular entanglement network to crystal-cross-linked network and crystal scaffold during film blowing of polyethylene: an *in situ* synchrotron radiation small- and wide-angle X-ray scattering study, *Macromolecules* 51 (2018) 4350–4362.
- [34] P. Hejmady, L.C. Cleven, L.C.A. van Breemen, P.D. Anderson, R. Cardinaels, A novel experimental setup for *in situ* optical and X-ray imaging of laser sintering of polymer particles, *Rev. Sci. Instrum.* 90 (2019), 083905.
- [35] J. Fang, W.R. Burghardt, R.A. Bubeck, *In situ* X-ray scattering measurements and polydomain simulations of molecular orientation development during injection molding of liquid crystalline Polymers, in: XV International Congress on Rheology, 2008, pp. 39–41.

- [36] S. Rendon, J. Fang, W.R. Burghardt, R.A. Bubeck, An apparatus for *in situ* x-ray scattering measurements during polymer injection molding, *Rev. Sci. Instrum.* 80 (2009), 043902.
- [37] B. Yang, R. Xia, J.B. Miao, J.S. Qian, M.B. Yang, P. Chen, Probing solidification kinetics of high-density polyethylene during injection molding using an in-situ measurement technique, *Polym. Test.* 32 (2013) 202–208.
- [38] B. Yang, G.J. Li, M.B. Yang, L.F. Su, J.B. Miao, R. Xia, P. Chen, S.Q. D, J.S. Qian, The Use of an *in-situ* measurement to probe the solidification kinetics of injection- molded HDPE-PP blends, *J. Res. Updates Polym. Sci.* 2 (2013) 1–7.
- [39] G. Andrieux, J.C. Eloy, E. Mounier, Technologies and market trends for polymer MEMS in microfluidics and lab-on-chip, *Proc. SPIE-Int. Soc. Opt. Eng.* 5718 (2005) 60–64.
- [40] C. Liu, Recent developments in polymer MEMS, *Adv. Mater.* 19 (2007) 3783–3790.
- [41] B.R. Whiteside, M.T. Martyn, P.D. Coates, *Precision Injection Molding: Process, Materials, and Applications*, Hanser, 2006, pp. 239–264.
- [42] M.W. Fu, W.L. Chan, A review on the state-of-the-art microforming technologies, *Int. J. Adv. Manuf. Technol.* 67 (2012) 2411–2437.
- [43] B.R. Whiteside, M.T. Martyn, P.D. Coates, G. Greenway, P. Allen, P. Hornsby, Micromoulding: process measurements, product morphology and properties, *Plast. Rubber Compos.* 33 (2013) 11–17.
- [44] Z. Lu, K.F. Zhang, Morphology and mechanical properties of polypropylene micro- arrays by micro-injection molding, *Int. J. Adv. Manuf. Technol.* 40 (2008) 490–496.
- [45] C. Yang, X.H. Yin, G.M. Cheng, Microinjection molding of microsystem components: new aspects in improving performance, *J. Micromech. Microeng.* 23 (2013), 093001.
- [46] S.Y. Yang, S.C. Nian, S.T. Huang, Y.J. Weng, A study on the micro-injection molding of multi-cavity ultra-thin parts, *Polym. Adv. Technol.* 22 (2011) 891–902.
- [47] Y. Pan, S. Shi, G. Zheng, W. Xu, K. Dai, C. Liu, J. Chen, C. Shen, Wide distribution of shish-kebab structure and tensile property of micro-injection-molded isotactic polypropylene microparts a comparative study with injection-molded macroparts, *J. Mater. Sci.* 49 (2014) 1041–1048.
- [48] T. Liao, X.T. Zhao, X. Yang, P. Coates, B. Whiteside, Z.Y. Jiang, Y.F. Men, Structural evolution of flow-oriented high density polyethylene upon heating: *In situ* SAXS and WAXD studies, *Polymer* 180 (2019), 121698.
- [49] T. Liao, X.T. Zhao, X. Yang, P. Coates, B. Whiteside, D. Barker, G. Thompson, Y. Q. Lai, Z.Y. Jiang, Y.F. Men, *In situ* synchrotron small angle X-ray scattering investigation of structural formation of polyethylene upon micro-injection molding, *Polymer* 215 (2021), 123390.
- [50] L. Balzano, Z. Ma, D. Cavallo, T.B. van Erp, L. Fernandez-Ballester, G.W.M. Peters, Molecular aspects of the formation of shish-kebab in isotactic polypropylene, *Macromolecules* 49 (2016) 3799–3809.
- [51] L.B. Li, W.H. De Jeu, Shear-induced smectic ordering as a precursor of crystallization in isotactic polypropylene, *Macromolecules* 36 (2003) 4862–4867.
- [52] J. Jiang, S.W. Wang, B. Sun, S.J. Ma, J.M. Zhang, Q. Li, G.H. Hu, Effect of mold temperature on the structures and mechanical properties of micro-injection molded polypropylene, *Mater. Des.* 88 (2015) 245–251.
- [53] G.R. Strobl, *The Physics of Polymers*, third ed., Springer, Berlin, Germany, 1997.
- [54] G.R. Strobl, M.J. Schneider, I.G. Voigtmartin, Model of partial crystallization and melting derived from small-angle X-ray-scattering and electron-microscopic studies on low-density polyethylene, *J. Polym. Sci., Part B: Polym. Phys.* 18 (1980) 1361–1381.
- [55] G.R. Strobl, M. Schneider, Direct evaluation of the electron-density correlation- function of partially crystalline polymers, *J. Polym. Sci., Polym. Phys. Ed.* 18 (1980) 1343–1359.
- [56] O. Glatter, O. Kratky, *Small Angle X-Ray Scattering*, Academic Press, London, UK, 1982.
- [57] N.S. Murthy, C. Bednarczyk, R.A.F. Moore, D.T. Grubb, Analysis of small-angle X- ray scattering from fibers Structural changes in nylon 6 upon drawing and annealing, *J. Polym. Sci., Part B: Polym. Phys.* 34 (1996) 821–835.
- [58] Z.Y. Jiang, Y.J. Tang, J. Rieger, H.F. Enderle, D. Lilge, S.V. Roth, R. Gehrke, Z. H. Wu, Z.H. Li, X.H. Li, Y.F. Men, Structural evolution of melt-drawn transparent high-density polyethylene during heating and annealing: synchrotron small-angle X-ray scattering study, *Eur. Polym. J.* 46 (2010) 1866–1877.
- [59] R. Perret, W. Ruland, Single and multiple X-ray small-angle scattering of carbon fibres, *J. Appl. Crystallogr.* 2 (1969) 209–218.
- [60] I. Lieberwirth, J. Loos, J. Petermann, A. Keller, Observation of shish crystal growth into nondeformed melts, *J. Polym. Sci., Part B: Polym. Phys.* 38 (2000) 1183–1187.
- [61] J. Petermann, M. Miles, H. Gleiter, The crystalline core of the row structures in isotactic polystyrene. I. Nucleation and growth, *J. Polym. Sci., Part B: Polym. Phys.* 17 (1979) 55–62.

- [62] M.X. Wang, W.B. Hu, Y. Ma, Y.Q. Ma, Orientational relaxation together with polydispersity decides precursor formation in polymer melt crystallization, *Macromolecules* 38 (2005) 2806–2812.
- [63] F.H. Liu, C. Guo, X. Wu, X.Y. Qian, H. Liu, J. Zhang, Morphological comparison of isotactic polypropylene parts prepared by micro-injection molding and conventional injection molding, *Polym. Adv. Met. Technol.* 23 (2012) 686–694.
- [64] M.R. Kantz, H.D. Newman, F.H. Stigale, The skin-core morphology and structure–property relationships in injection-molded polypropylene, *J. Appl. Polym. Sci.* 16 (1972) 1249–1260.
- [65] Y.M. Pan, S.Y. Shi, W.Z. Xu, G.Q. Zheng, K. Dai, C.T. Liu, J.B. Chen, C.Y. Shen, Wide distribution of shish-kebab structure and tensile property of micro-injection- molded isotactic polypropylene microparts: a comparative study with injection- molded macroparts, *J. Mater. Sci.* 49 (2013) 1041–1048.
- [66] P.H. Hermans, P. Platzek, The deformation mechanism and the fine structure of hydrate cellulose. IX. the theoretical relation between swelling anisotropy and the characteristic double refraction of orienten filaments, *Kolloid Z.* 88 (1939) 68–72. [67] M. Polanyi, The X-ray fiber digram, *Z. Phys.* 7 (1921) 149–180.
- [68] M. Rubinstein, R.H. Colby, *Polymers Physics*, Oxford University Press, New York, 2003.
- [69] X.T. Zhao, T. Liao, Y. Lu, Z.Y. Jiang, Y.F. Men, Formation and distribution of the mesophase in ultrasonic micro-injection- molded isotactic polypropylene, *Macromolecules* 54 (2021) 5167–5177.
- [70] L.J. Fetters, D.J. Lohsey, R.H. Colby, Chain Dimensions and Entanglement Spacings, *Physical Properties of Polymers Handbook*, 2006, pp. 447–454.
- [71] A. Frick, C. Stern, G. Michler, S. Henning, M. Ruff, Study on flow induced nano structures in iPP with different molecular weight and resulting strength behavior, *Macromol. Symp.* 294 (2010) 91–101.
- [72] S. Vleeshouwers, H.E.H. Meijer, A rheological study of shear induced crystallization, *Rheol. Acta* 35 (1996) 391–399.
- [73] R.H. Somani, B.S. Hsiao, A. Nogales, S. Srinivas, A.H. Tsou, I. Sics, F.J. Balta- Calleja, T.A. Ezquerra, Structure development during shear flow-induced crystallization of i-PP: *in-situ* small-angle X-ray scattering study, *Macromolecules* 33 (2000) 9385–9394.